Supporting Information

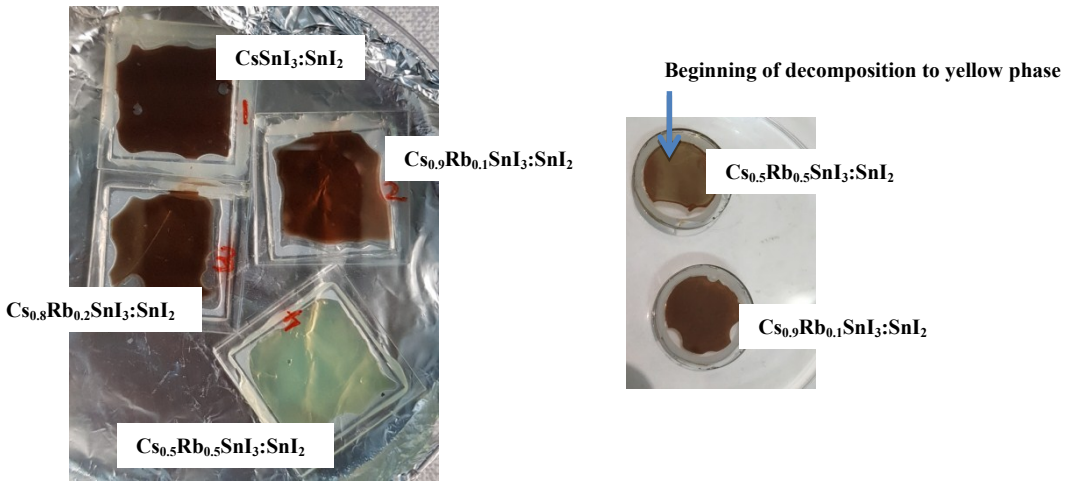

Figure S1: (a) Photograph of $Cs_{1-x}Rb_xSnI_3$ films (x = 0, 0.1, 0.2, 0.5) spin cast from 8 wt.% DMF solutions and encapsulated under nitrogen. Notably, even with encapsulation $Cs_{0.5}Rb_{0.5}SnI_3$ perovskite is unstable, decomposing to the yellow phase within hours/days.; **(b)** Photograph of $Cs_{0.9}Rb_{0.1}SnI_3$ and $Cs_{0.5}Rb_{0.5}SnI_3$ immediately after perovskite deposition and encapsulation under nitrogen. For the latter the start of degradation to the yellow phase is evident. All perovskite films were deposited with 10 mol% SnI_2 as a source of excess Sn.

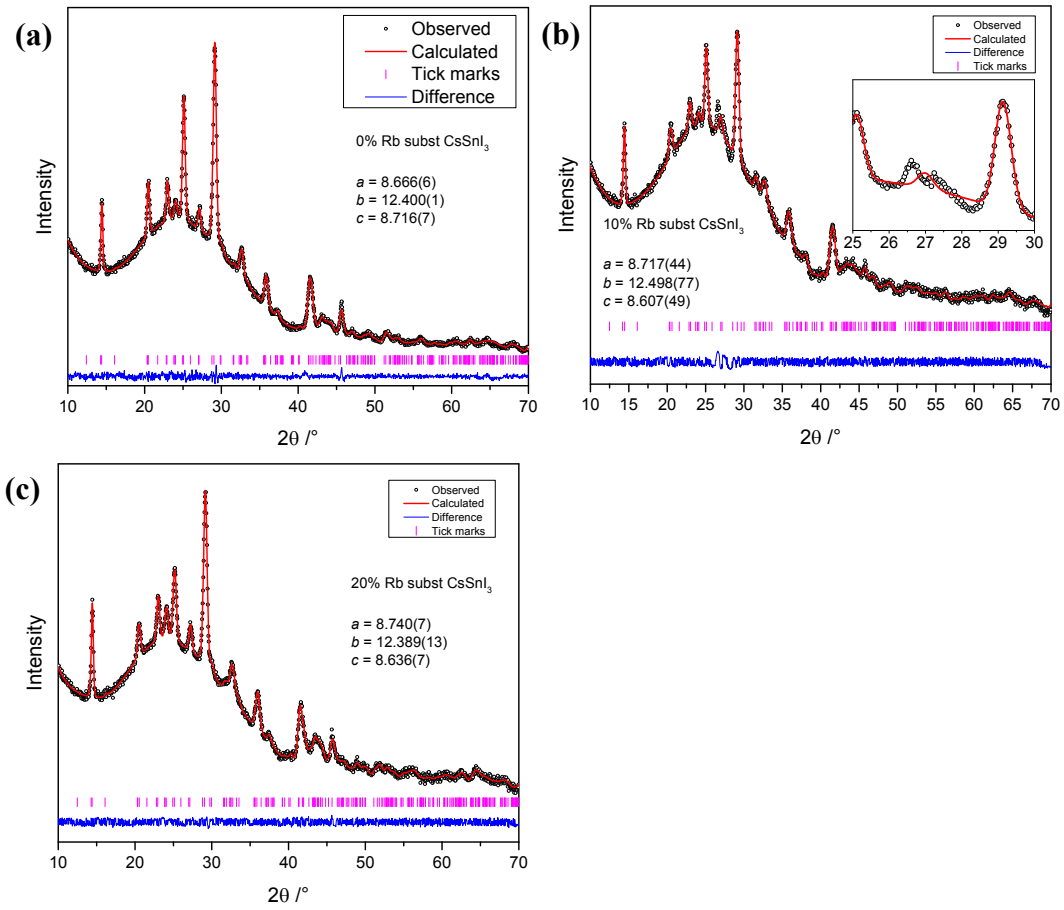

Figure S2: Lattice parameter fitting using space group *Pnma* of XRD patterns of $Cs_{1-x}Rb_xSnI_3$ where x = 0 **(a)**, 0.1 **(b)** (inset shows presence of possible impurity phase), or 0.2 **(c)**. The lattice parameters shown on the graphs have units of Ångströms.

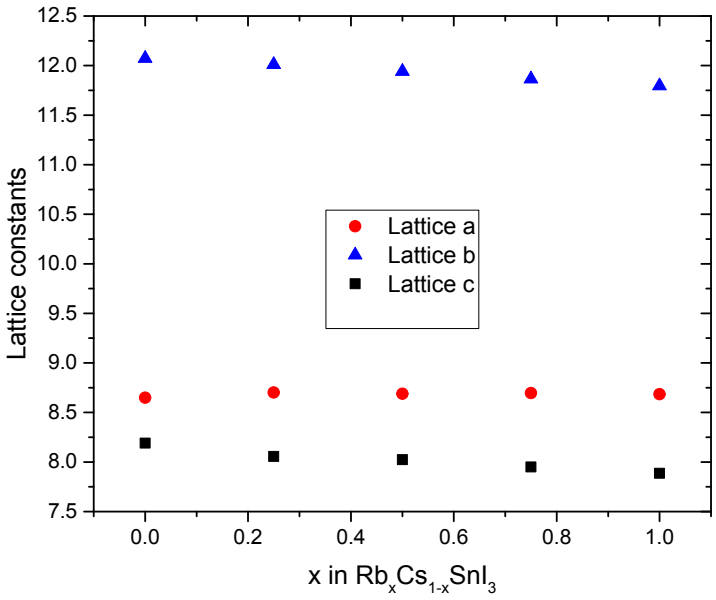

Figure S3: Calculated lattice constants evolution with increasing Rb in orthorhombic $Cs_{1-x}Rb_xSnI_3$ (in Å).

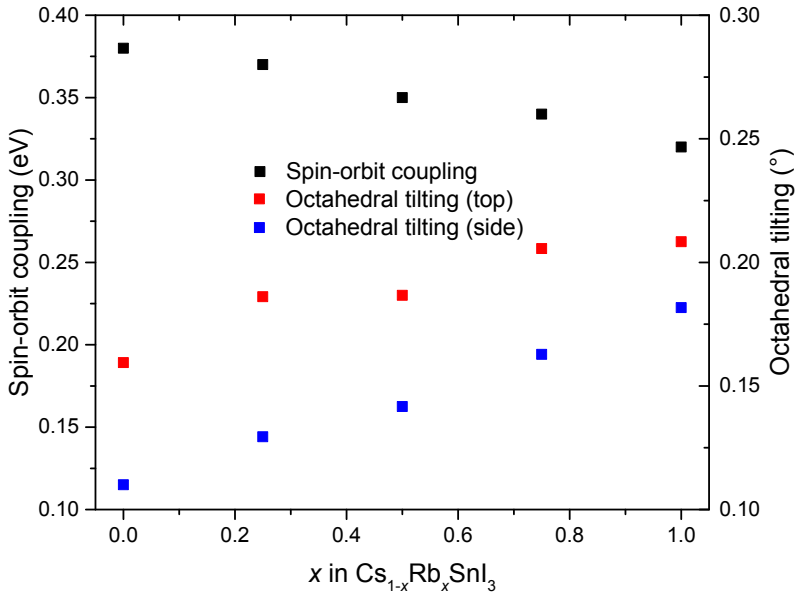

Figure S4: Calculated average octahedral tilting angles and the corresponding spin-orbit coupling effect derived from DFT-1/2 calculated band gaps with and without the spin-orbit coupling effect.

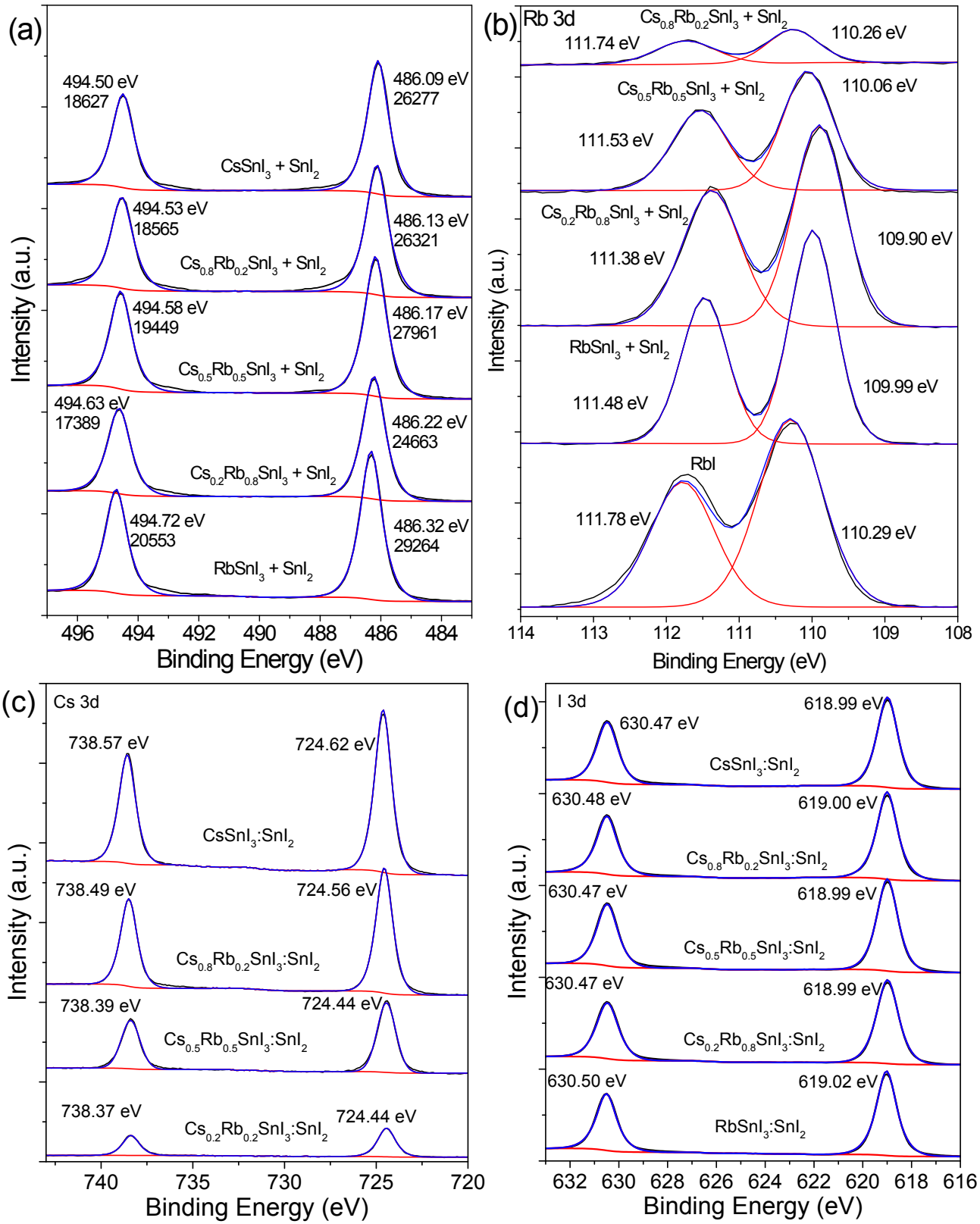

Figure S5: XPS spectra of $Cs_{1-x}Rb_xSnI_3$ + 10 mol% SnI_2 where x = 0, 0.2, 0.5, 0.8, and 1, showing **(a)** Sn 3d; **(b)** Rb 3d; **(c)** Cs 3d; **(d)** I 3d. Also shown in (b) is the binding energy for Rb 3d in RbI.

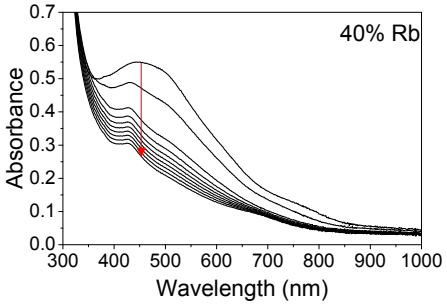

Figure S6: Electronic absorption spectra of $Cs_{0.6}Rb_{0.4}SnI_3$:SnI_2 taken over time exposed to ambient air. Measurements were taken every 5 minutes

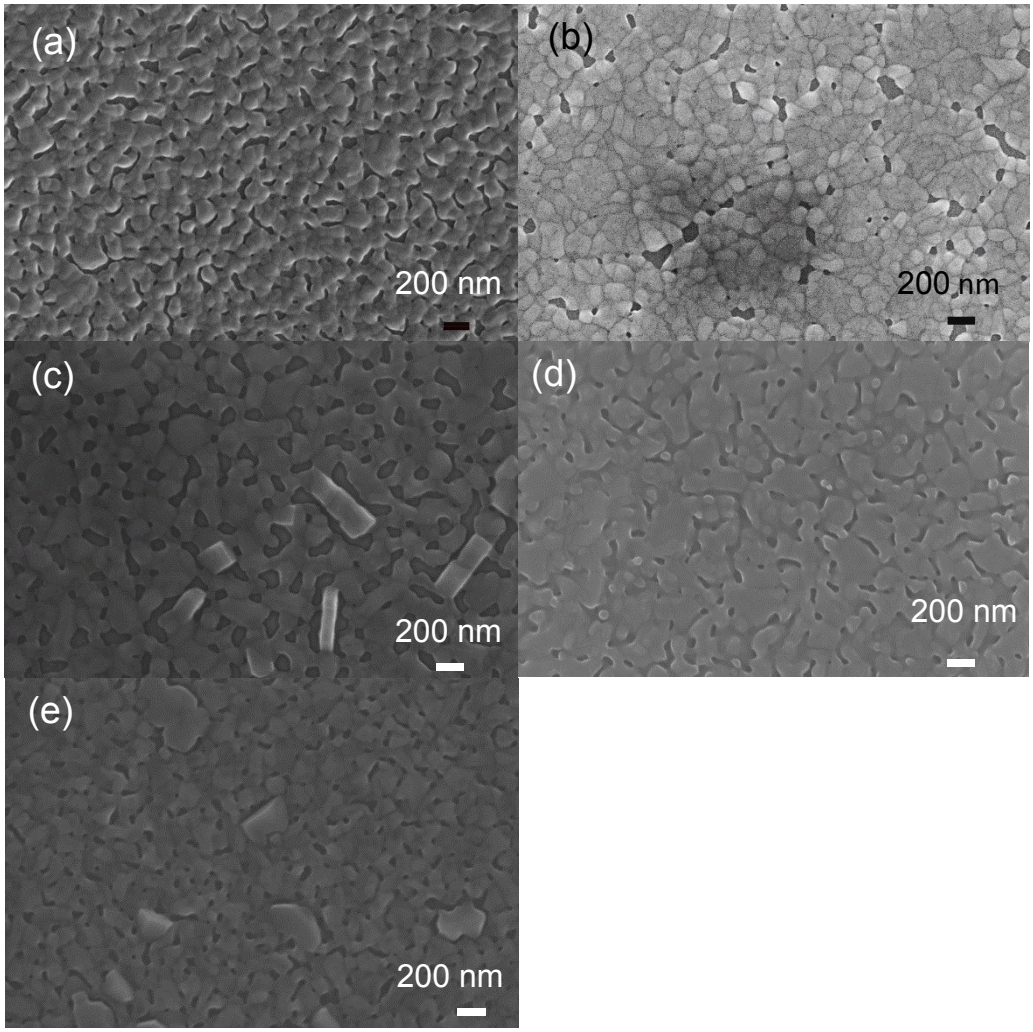

Figure S7: SEM image of a film of: **(a)** $Cs_{0.8}Rb_{0.2}SnI_3$:SnI_2 (~6%) **(b)** $CsSnI_3$:SnI_2 (~1.6%) **(c)** $Cs_{0.5}Rb_{0.5}SnI_3$:SnI_2 (15.9%) **(d)** $Cs_{0.8}Rb_{0.2}SnI_3$:$SnCl_2$, (4.3%) and **(e)** $Cs_{0.5}Rb_{0.5}SnI_3$:$SnCl_2$ (6.8%) on an ITO glass substrates. For each image the values in brackets correspond to the area of the substrate not covered by the perovskite film.

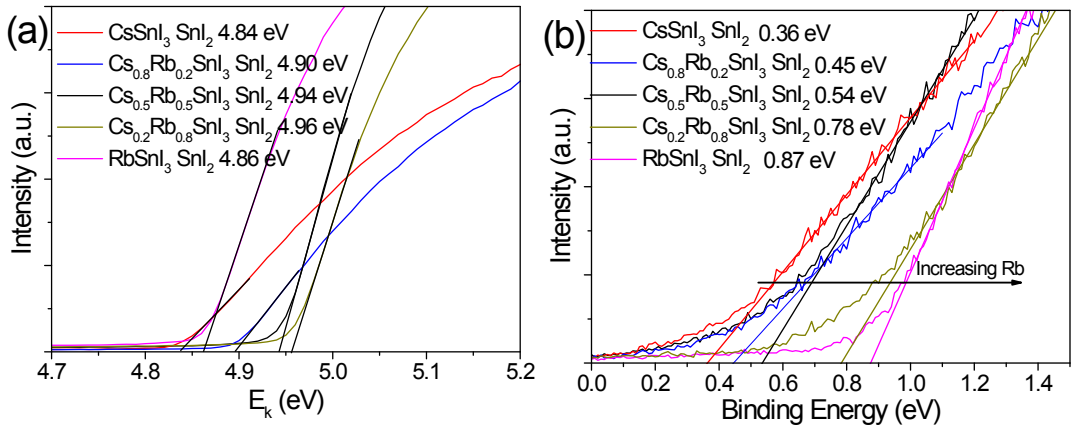

Figure S8: UPS of $Cs_{1-x}Rb_xSnI_3$, where x = 0, 0.2, 0.5, 0.8 and 1, showing **(a)** low kinetic energy cut-off and **(b)** high kinetic energy cut-off. The ionisation potential is equal to the sum of the work function (deduced from the secondary electron cut-off in (a)) and the difference in energy between the Fermi level (binding energy = 0) and valance band edge deduced from (b).

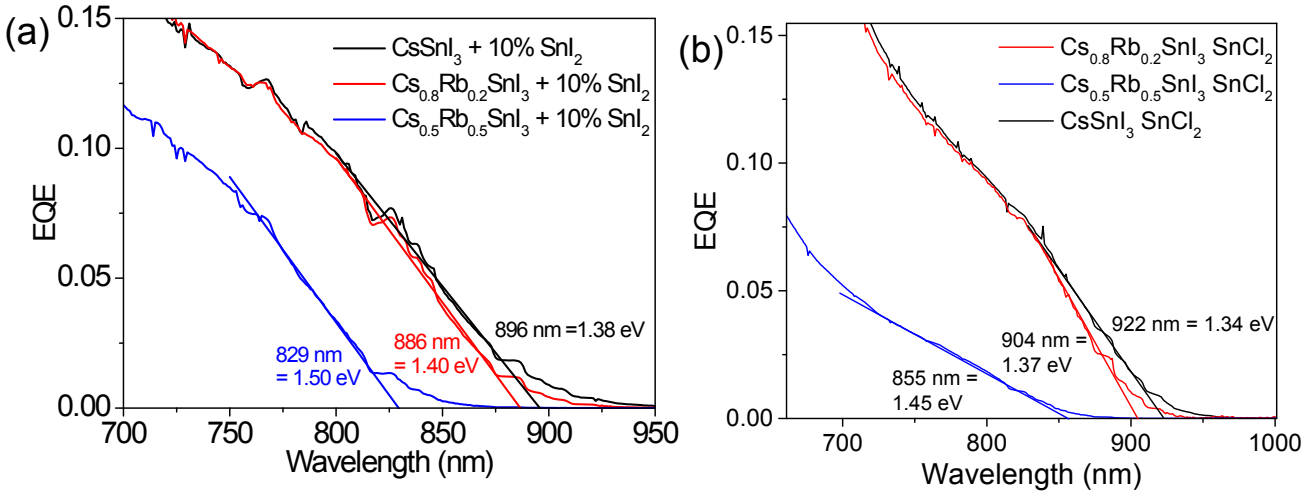

Figure S9: Low energy edge of EQE spectra shown in Figure 7(b) and 8(b) of main manuscript: **(a)** ITO| $Cs_{1-x}Rb_xSnI_3$:SnI_2| C_{60}| BCP| Al, and **(b)** ITO| $Cs_{1-x}Rb_xSnI_3$:$SnCl_2$| $PC_{61}BM$| BCP| Al.

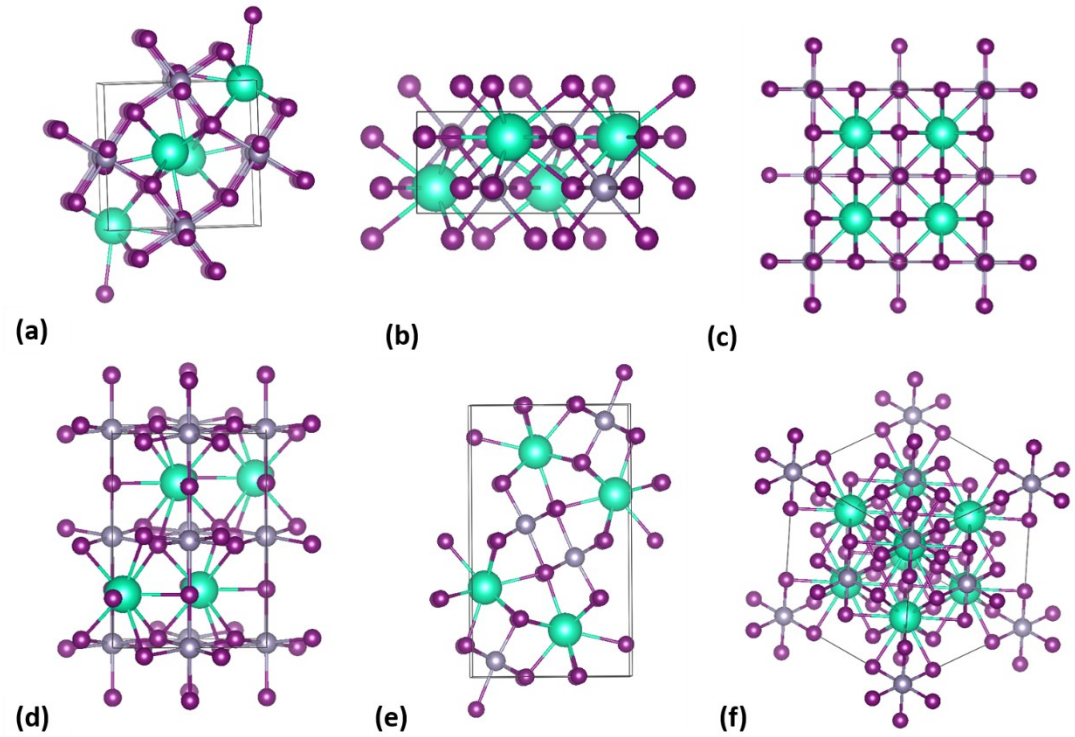

Figure S10: Top (a, b, and c) and side (e, f, and g (45 degree tilting)) views of orthorhombic, yellow phase $CsSnI_3$ and FCC Cs_2SnI_6. Figures are made using VESTA[a]. Purple, green, and grey spheres denote I, Cs and Sn, respectively.

Table S1: Relative proportions of Cs and Rb estimated from the XPS $3d_{5/2}$ + $3d_{3/2}$ peak intensities using the relative sensitivity factors for Cs and Rb 3d peaks, 40.22 and 4.21 respectively.

Sample	**Cs / %**	**Rb / %**
$Cs_{0.8}Rb_{0.2}SnI_3$:SnI_2	80.1	19.9
$Cs_{0.5}Rb_{0.5}SnI_3$:SnI_2	43.5	56.5
$Cs_{0.2}Rb_{0.8}SnI_3$:SnI_2	15.0	85.0

Table S2: Summary of JV characteristics of PV devices made using $CsSnI_3$ + 10 mol% SnI_2 with 0, 20% or 50% Cs substituted for Rb, and a C_{60} ETL.

Sample	n	J_{sc} (mA/cm^2)	V_{oc} (V)	*FF*	η (%)	Champion η (%)
$CsSnI_3$:SnI_2	18	9.84 ± 0.67	0.31 ± 0.01	0.46 ± 0.02	1.37 ± 0.14	1.55
$Cs_{0.8}Rb_{0.2}SnI_3$:SnI_2	17	8.79 ± 0.25	0.43 ± 0.02	0.45 ± 0.01	1.70 ± 0.09	1.84
$Cs_{0.5}Rb_{0.5}SnI_3$:SnI_2	18	8.11 ± 0.53	0.48 ± 0.04	0.46 ± 0.05	1.81 ± 0.30	2.25

Table S3: JV characteristics of PPV devices in the structure ITO| $Cs_{1-x}Rb_xSnI_3$ + 10 mol% $SnCl_2$| $PC_{61}BM$| BCP| Al, immediately after fabricating (black), after 5 days (red) and 12 days (blue) storage in an N_2 filled glovebox.

Sample	n	J_{sc} (mA/cm^2)	V_{oc} (V)	*FF*	η (%)	Champion η (%)
$CsSnI_3$:$SnCl_2$	16	5.32 ± 0.78	0.37 ± 0.01	0.57 ± 0.04	1.14 ± 0.24	1.50
	15	5.30 ± 0.79	0.41 ± 0.02	0.61 ± 0.02	1.33 ± 0.26	1.67
	14	5.33 ± 0.97	0.44 ± 0.01	0.62 ± 0.03	1.46 ± 0.34	1.98
$Cs_{0.8}Rb_{0.2}SnI_3$:	17	6.71 ± 0.71	0.50 ± 0.01	0.61 ± 0.03	2.05 ± 0.26	2.58
$SnCl_2$	16	6.42 ± 0.63	0.48 ± 0.09	0.60 ± 0.14	1.93 ± 0.64	2.64
	16	6.75 ± 0.68	0.48 ± 0.02	0.67 ± 0.02	2.19 ± 0.20	2.45
$Cs_{0.5}Rb_{0.5}SnI_3$:	18	2.18 ± 0.17	0.53 ± 0.02	0.44 ± 0.03	0.50 ± 0.07	0.63
$SnCl_2$	16	2.22 ± 0.17	0.54 ± 0.01	0.58 ± 0.01	0.70 ± 0.06	0.79
	17	2.31 ± 0.17	0.53 ± 0.01	0.60 ± 0.02	0.74 ± 0.07	0.90